Materials Physics and Mechanics. 2023;51(4): 142-159
Research article
http://dx.doi.org/10.18149/MPM.5142023_13

Submitted: November 24, 2022
Approved: December 19, 2023
Accepted: January 30, 2023

The effect of mass collapse under hypervelocity impact of solid paraboloid into a thin screen

A.F. Nechunaev, N.V. Naumova, N.P. Dorofeev ✉

St. Petersburg State University, St. Petersburg, Russia

✉ nickdorof60@gmail.com

Abstract. In this article, an impact of a solid-paraboloid at a speed of 4190 m/s into a thin aluminum plate is numerically simulated. Such high-speed impacts are dangerous as they can damage the second screen of the Whipple shield. Whipple shield, so-called dual-wall system, is widely used to protect spacecraft from space debris. This paper reviews the mechanism of the interaction between the projectile and bumper, the movement and diffusion of the debris cloud. Numerical simulation for high-speed impact of a hyperboloid on an aluminum alloy plate is presented. Central and non-central impacts are discussed. It is shown that some types of collisions are very dangerous because significant mass of fragments is concentrated on the impact axis. The same calculations were conducted for the sphere of comparable mass, results were compared.

Keywords: hypervelocity impact; space debris; mass collapse effect

Citation: Nechunaev AF, Naumova NV, Dorofeev NP. The effect of mass collapse under hypervelocity impact of solid paraboloid into a thin screen. *Materials Physics and Mechanics*. 2023;51(4): 142-159. DOI: 10.18149/MPM.5142023_13.

Introduction

With the development of human space activities, the volume of technogenic space debris in orbits of different heights is rapidly progressing. As of 2021, more than 130 million objects with a size of 0.1-1 cm are known [1]. Among them: spent rocket stages, fragments from the collision of satellites, particles covering spacecraft, particles of rocket fuel, and other debris. If particles collide with a spacecraft at velocities exceeding 4-7 km per second, they can cause irreversible destruction of the covering, depressurization or damage expensive devices and mechanisms.

Usually, to protect a spacecraft against hypervelocity impacts, so-called Whipple shield is used [2]. When a dangerous particle collides with the first screen of Whipple shield, fragments of a spherical- or pear-shape form a cloud and move to the second screen of Whipple shield [3]. The impact of a debris cloud on the second Whipple shield is less dangerous than the impact of a compact projectile.

Methods for modeling such interactions are well known. Among them: SPH method (smoothed-particle hydrodynamics) [4–16], the discrete elements method [17,18], the finite element method [19–21]. As the velocities of both one SPH particle and a group of such particles have often been studied, we will focus on the SPH method.

In the paper, numerical simulation was conducted using SPH method (smoothed-particle hydrodynamics). This method is successfully used to simulate significant displacements and deformations not only on low-velocity interactions (100-1000 m/s), but, as was shown in [24–26], on interactions at higher speeds. For creating a geometry of SPH-bodies and defining

material models, preprocessor LS-Pre-Post was used [19]. As a solver we used a widely known software package ANSYS/LS-DYNA.

Methods

The first phase of a given study is to test simulation parameters at a speed of, 4190 m/s. This was achieved by comparing results of numerical simulation with the results of the experiment – "two-stage light gas guns" according to Fa-wei Ke and others [22]. Numerical simulation was made for the impact of a sphere out of Al-1100 against a thin Al-6061-T6 aluminum plate with the speed given above. Sphere diameter matched the diameter of the sphere studied in the experiment and was equal to 5.01 mm. Thicknesses of the plates were also identical and were 1 mm. During simulation, the plate was supported by a fixed ring (Fig. 1).

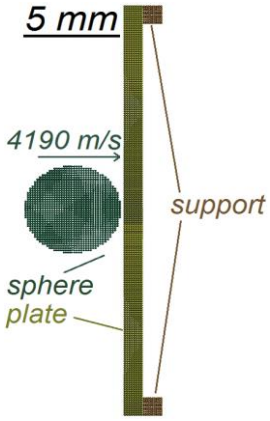

Fig. 1. Problem statement for verification of model's parameters. High velocity impact of a sphere against a thin plate. Plane cut along the main axis of a model is shown

Figures 2 and 3 show the resulting debris clouds at 16 and 24 microseconds times of impact. Computational simulations with the parameters shown in Tables 1-3 show good agreement with the experiment of author Fa-wei Ke and other scientists, who carried out the fixation of the debris cloud evolution with laser shadowgrams. The ratio of fragment cloud length to maximum cloud diameter is 1.58 for the computational simulation and 1.53 for the experiment at a time of 16 microseconds. Accordingly, a discrepancy of about 3.5 % with the experiment was obtained. At the time point of 24 microseconds, this ratio is 1.58 for the computational modelling and 1.59 for the experiment. Correspondingly, the discrepancy with the experiment was 0.5 % [23].

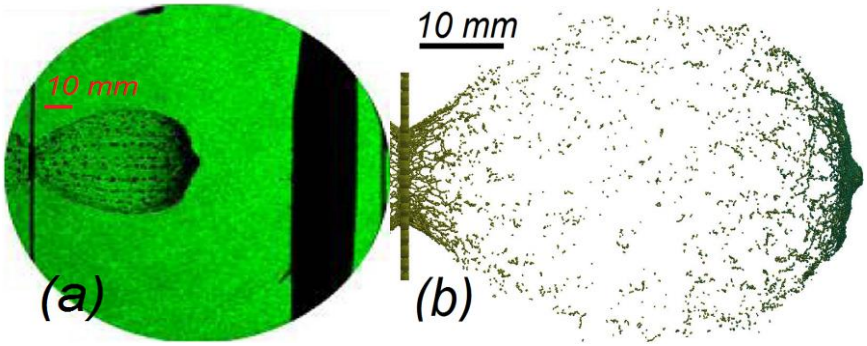

Fig. 2. View of the cloud of fragments at a time of 16 μs after the impact: (a) – experiment by F. Ke and other scientists [22]; (b) – numerical simulation. Initial impact velocity was V = 4190 m/s, sphere material is Al-1100, sphere diameter is 5.01 mm, barrier material is Al-6061-T6, h = 1 mm

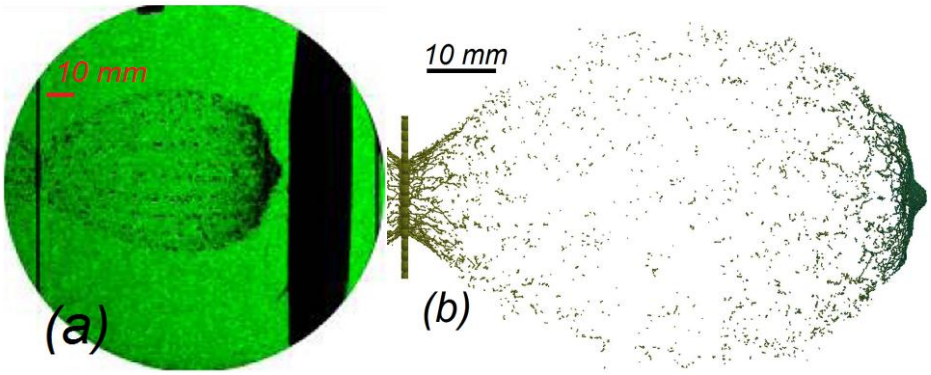

Fig. 3. View of the cloud of fragments at 24 μs after the impact: (a) – experiment according to Fa. Ke and other scientists [22]; (b) – numerical simulation. Initial impact velocity was V = 4190 m/s, sphere material is Al-1100, sphere diameter is 5.01 mm, barrier material is Al-6061-T6, h = 1 mm

Table 1. Materials' Constants and Parameters [22]

Parameter	Unit.	*Al-1100*	*Al 6061-T6*
Density ρ	kg/m^3	2770	2750
Modulus of shearing G	Pa	25.9×10^9	25×10^9
Yield stress A	Pa	4.1×10^7	3.241×10^8
Material hardening B	Pa	1.25×10^8	1.138×10^8
exponent n	-	0.183	0.42
Johnson-Cook constant c		0.001	0.002
Thermodynamic parameter m		0.859	1.34
Testing temperature	K	293	293
Melting temperature	K	893	893
Testing strain rate	1/s	1	1
Specific heat capacity, C_p	J/(kg·K)	910	910
Coefficients in the Johnson-Cook destruction model D_1		0.071	-0.77
D_2		1.248	1.45
D_3		-1.142	-0.47
D_4		0.0097	0
D_5		0	1.6

Table 2. Linear polynomial equation of state coefficients [22]

C_0	C_1, GPa	C_2, GPa	C_3, GPa	C_4	C_5	C_6	E_0	V_0
0	74.2	60.5	36.5	1.96	0	0	0	1

Table 3. Mie-Gruneisen equation of state coefficients [22]

C_0, m/s	S_1	S_2	S_3	a	E_0	Γ_0	V_0
3935	1.578	0	0	0	0	1.69	1

In the second stage of the present study, a computational simulation of a high-speed impact of a solid paraboloid of rotation, the geometrical dimensions of which are shown in Fig. 5, with a similar initial velocity V = 4190 m/s was performed. The geometric dimensions of the solid-paraboloid were chosen so that the number of particles, and thus the mass of the paraboloid, were comparable with the dimensions and mass of the sphere from the first stage of the present study.

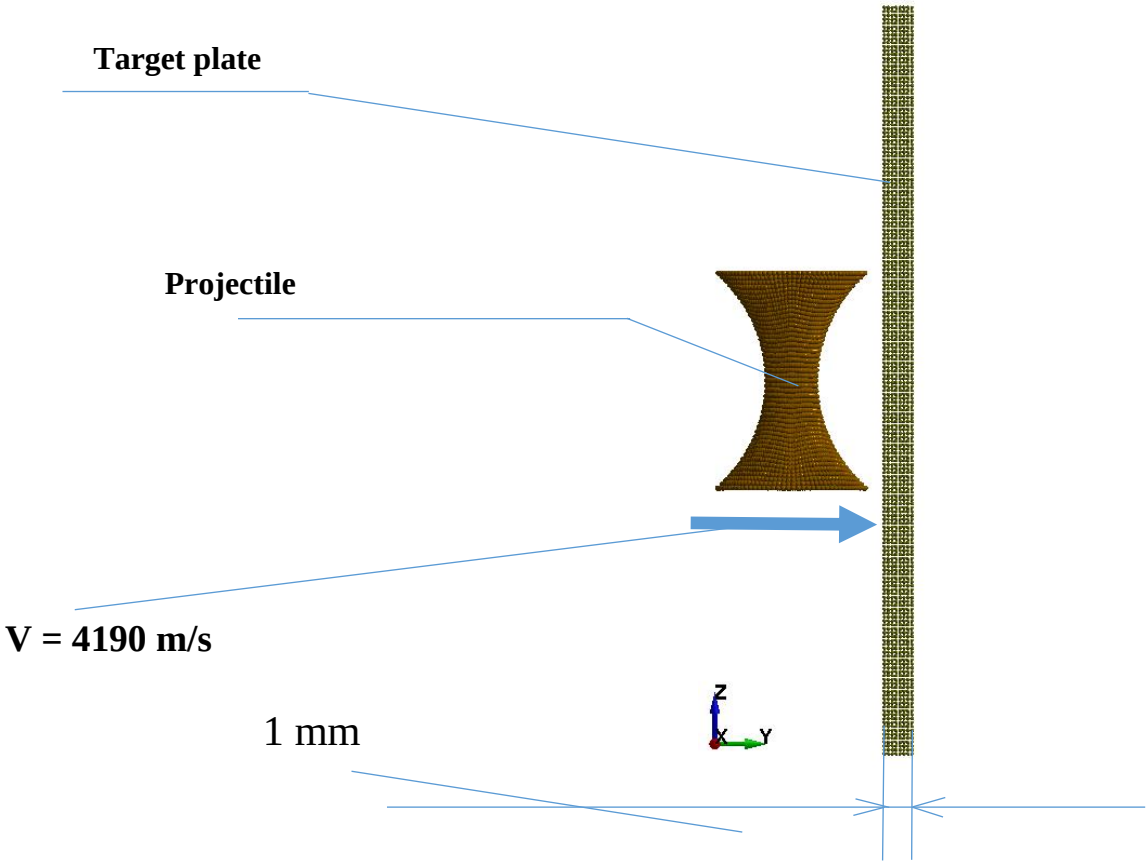

Fig. 4. Problem statement. Solid paraboloid of rotation material is Al. Barrier material is Al-6061-T6, h =1 mm.

The number of SPH particles of the shock (rotational paraboloid) was 41000. For comparison, the number of SPH particles of the sphere from the first stage of this study was 33000. A 3D view of the computational model before the calculation, which does not show the reference ring, is shown in Fig. 6.

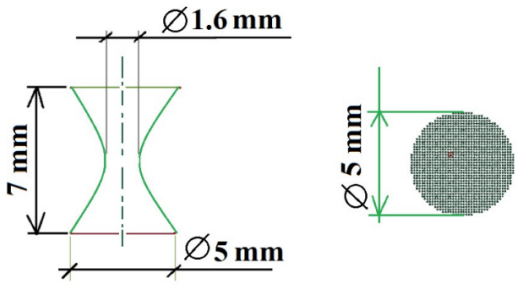

Fig. 5. Comparison of the sphere from the first phase of the study with the solid paraboloid of rotation

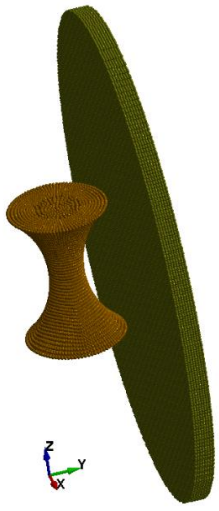

Fig. 6. 3D view of the model

The calculated mass of the aluminum sphere considered in the first stage of this study was 183 mg. The mass of the rotation paraboloid was 119.7 mg at Preprocessor Ls-Pre-Post.

Figure 7 shows the evolution of the debris cloud during the interaction of a solid-paraboloid of rotation with a thin 1-mm plate at time moments t = 0, 1.7, 3.4, and 5.5 μs.

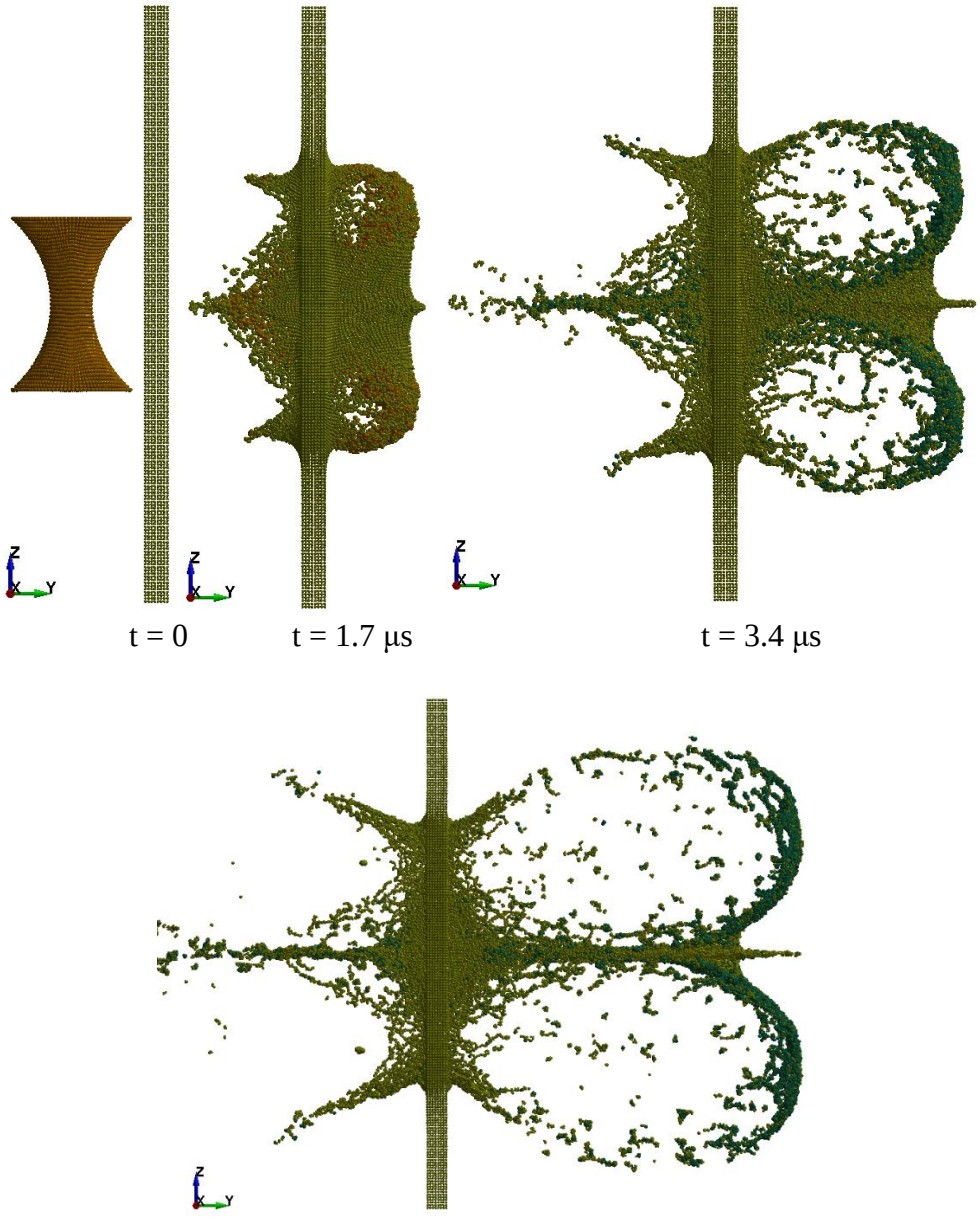

Fig. 7. Evolution of the debris cloud after solid paraboloid of rotation strikes aluminum thin 1-mm plate

At 5.5 μs (Fig. 7) we can clearly observe that oval clouds' velocity became equal to velocity of a central "spike-like" cloud which is located on the impact axis and leads to faster evolution of these clouds compared to central SPH-particles.

In the next step of the computational modelling, we will carry out the calculation of the mass of the "spike". The "spike" consisting of SPH particles is highlighted by the red box in Fig. 8. The mass of sphere from the first stage of the study is 183 mg, which is informatively given by the LS-Pre-Post preprocessor. Then the mass of 1 SPH particle is

183 mg / 33000 = 0.00555 mg. In the "spike" 34,188 particles were isolated. Then the mass of the spike = 190 mg (that is 34188 multiplied by 0.00555). I.e. the mass of the spike in this problem is comparable to the mass of the sphere from the first step.

Conclusion: Normal impact of solid paraboloid of rotation is as dangerous for the second screen of Whipple shield (after passing through the first one). This is clearly visible in the Figs. 8 and 10 (shape of the cloud of fragments at t = 10.6 μs (view from above)).

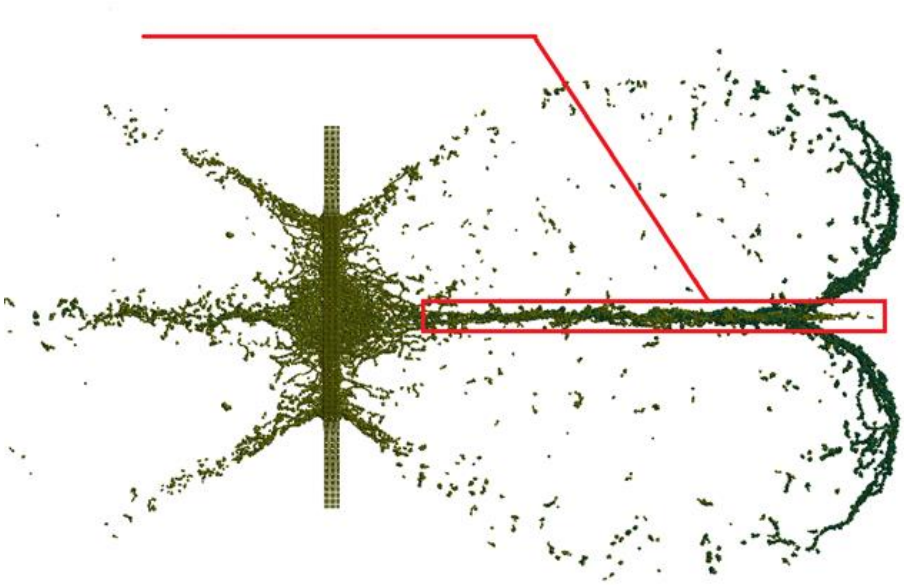

Fig. 8. Time t = 10.6 μs. Region of SPH particles is selected to estimate number of particles

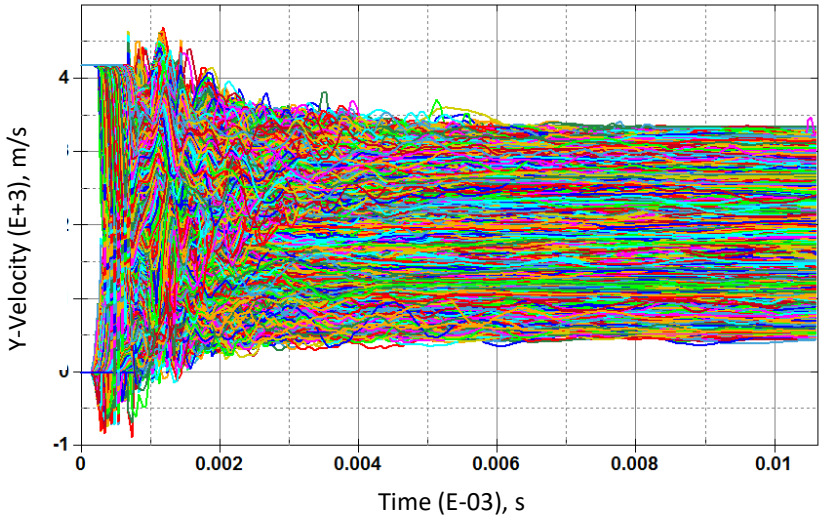

Fig. 9. Group diagram of particles' velocities inside the spike

Group diagram (Fig. 9) shows velocity spectrum of particles located inside the "spike" starting from ~ 400 m/s and ending with ~ 3300 m/s. This group diagram provides clear image that some particles came to the "spike" from the striker (initial velocities at t = 0 from 4190 m/s mark, while some of them were in a state of rest - V = 0 m/s at t = 0). After 6 μs cloud motion stabilizes, wave oscillations of the particles' velocities reduce and eventually disappears – curves of the velocities of particles are practically parallel to x-axis.

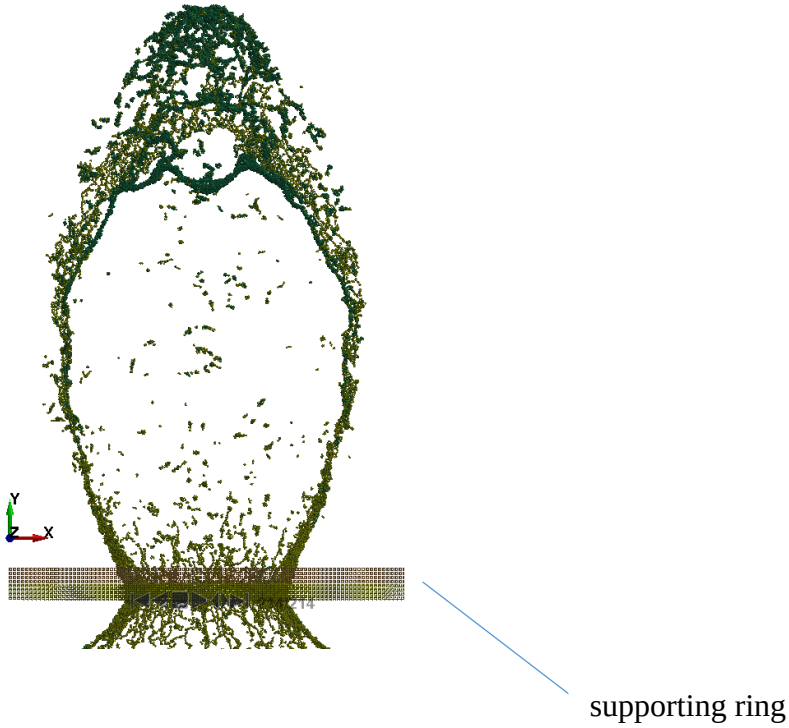

Fig. 10. Shape of the cloud of fragments at t = 10.6 μs (view from above)

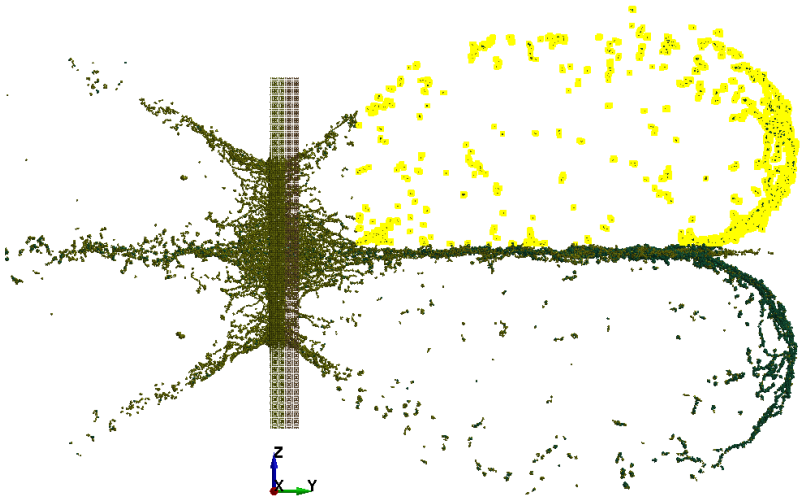

Fig. 11. Top cloud particles selection (shown in yellow) to calculate mass of the cloud

Let us establish the number of particles in each cloud (Fig. 11). This would be 11563 SPH. Given that there are 34,000 particles concentrated in the center (spike), we conclude that each cloud is low hazard, especially since the impact in the second Whipple shield screen would be a "spot" rather than a point impact.

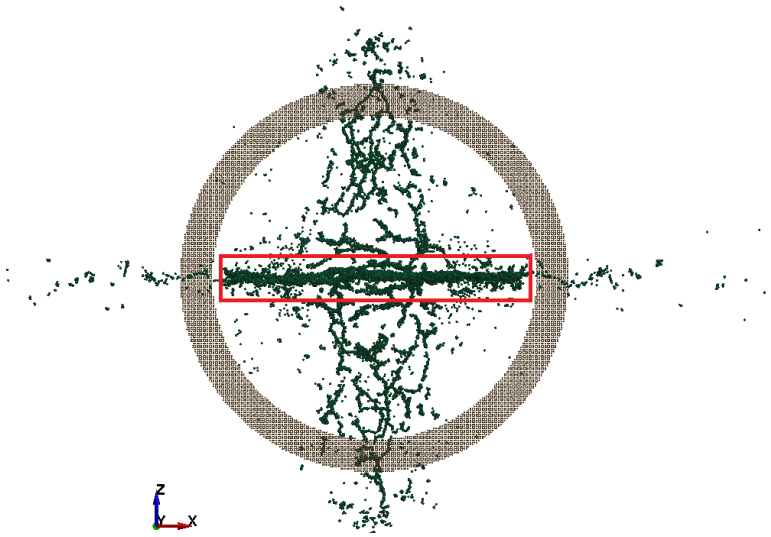

Fig. 12. Dangerous vanguard of clouds, view from the front

During the third step of the study let us split the cloud of debris, formed after the impact of paraboloid, into speed zones.

Zone 1. Low speed zone (near the impact axis, simultaneously it is located right after free surface of a barrier).

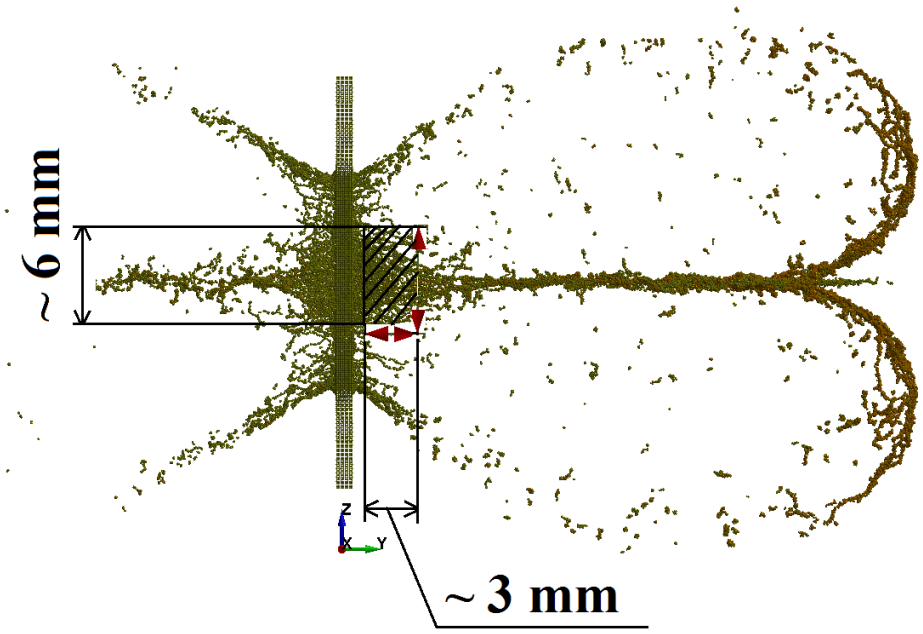

Fig. 13. Selection of SPH particles from the low velocity zone 1 to establish a picture of evolution of debris clouds at t = 10 μs. Zone 1 is hatched. Supporting ring is hidden

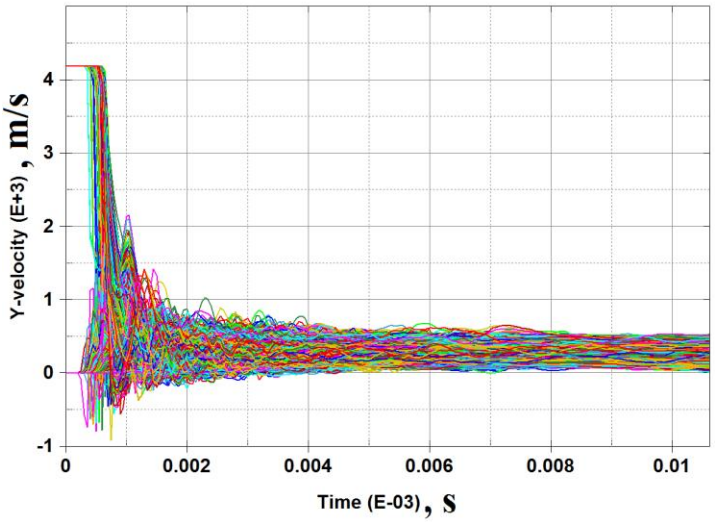

Fig. 14. Velocity diagram of cloud of fragments from low-speed zone

Zone 2. Medium velocity area (in proximity to the impact axis, located between low-velocity area 1 and high-velocity area 3).

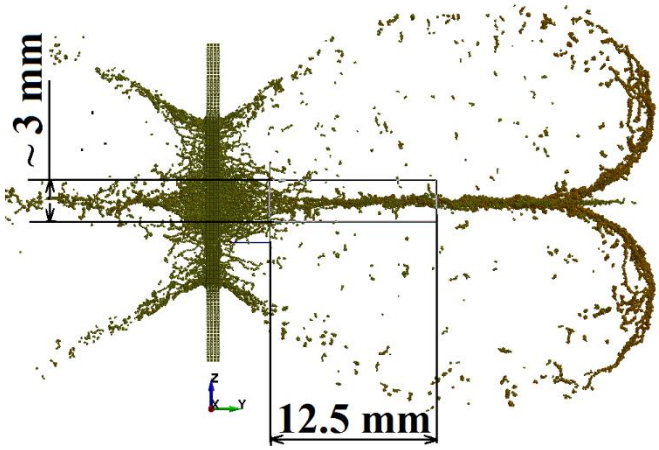

Fig. 15. Selection of SPH particles from medium-speed zone 2 to define a shape of evolution of the debris cloud at t = 10 μs. Supporting ring is hidden

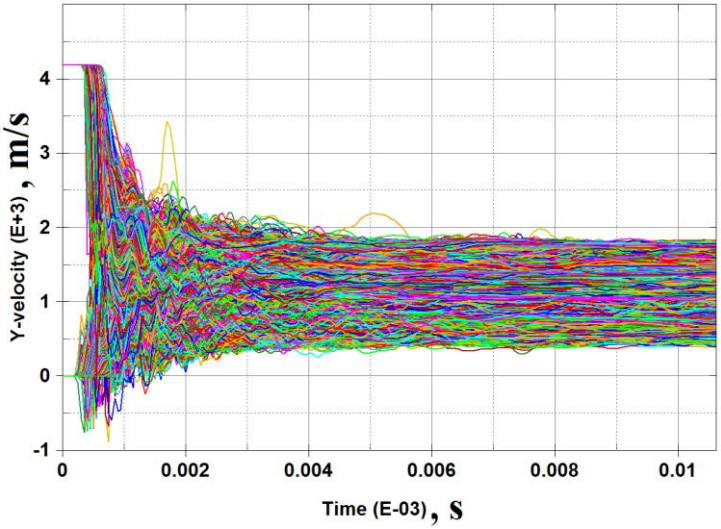

Fig. 16. Velocity diagram of debris cloud from medium-speed area

We consider low-velocity area to be an area with particle velocities varying from 0 m/s to 500-600 m/s. Particles from this zone are scattered and do not have any effect on the integrity of the second screen of Whipple shield. Dimensions of a rectangle which contain low-velocity area are shown in Fig. 13, a velocity diagram of this area is presented in Fig. 14. Dimensions of a rectangle which contain medium-velocity area are shown in Fig. 15, a velocity diagram of this area is presented in Fig. 16. Figure 16 indicates that, velocity of particles located in this zone does not exceed 2 km/s and do not pose a substantial threat in space in case of a relatively small mass of particles (fragments). We base our conclusions on findings of [28]. It states that maximum velocity of collision of a striker against a barrier exists. If collision occurs at a higher velocity and the striker penetrates the barrier, the deformation of a striker of any form is accompanied by fluidity. For ordinary materials, evidently, this maximum speed has an order of magnitude of 2 km/s.

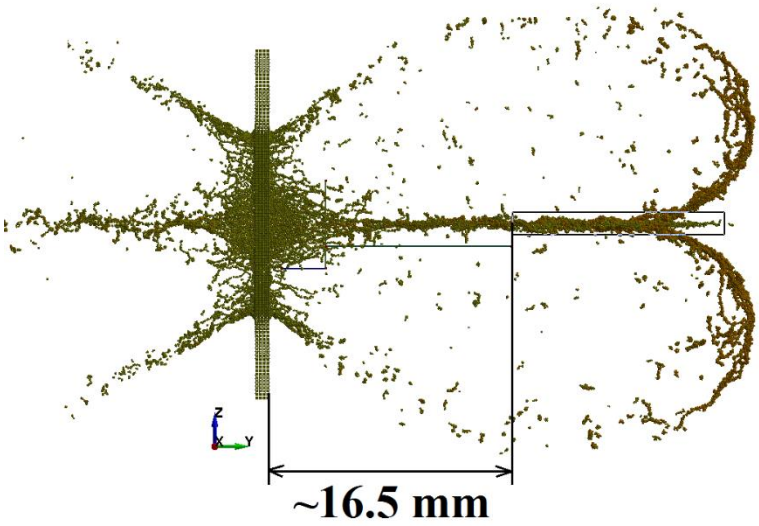

Fig. 17. Selection of SPH particles from high-speed zone 3 to define a shape of evolution of the debris cloud at t = 10 μs. Supporting ring is hidden

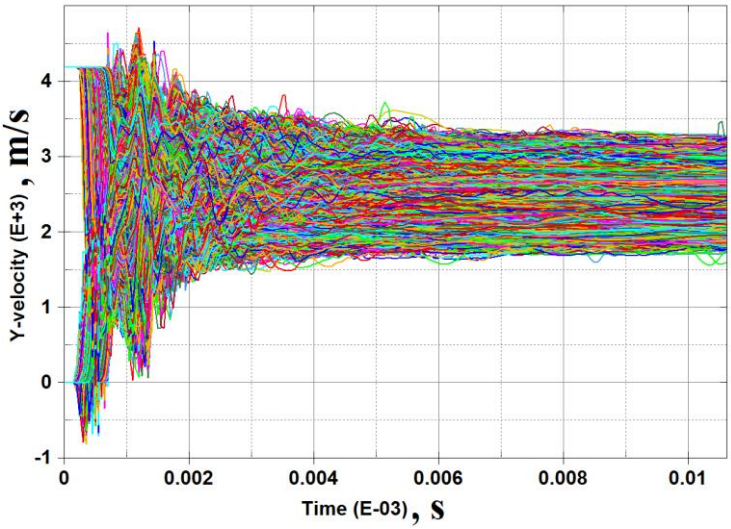

Fig. 18. Velocity diagram of cloud of fragments from high-speed area

Zone 3. High velocity area (in proximity to the impact axis, the most remote area from the barrier surface). Choice of this zone is shown in Fig. 17. The rectangle height along Z in this case is ~ 1.5 mm. The velocity diagram of particles from this zone, presented in Fig. 18, indicates that particles located in the "spike" of the cloud have velocities varying from 1700 m/s to 3300 m/s.

Let us examine the case of diverted impact of a paraboloid when the velocity vector is at an angle of 5, 30 and 45 degrees to barrier normal (cases 1 – 6) to estimate the danger of these cases for the second screen of Whipple shield.

Case 1. Velocity vector of paraboloid is at an angle of 5 degrees to barrier normal (Fig. 19).

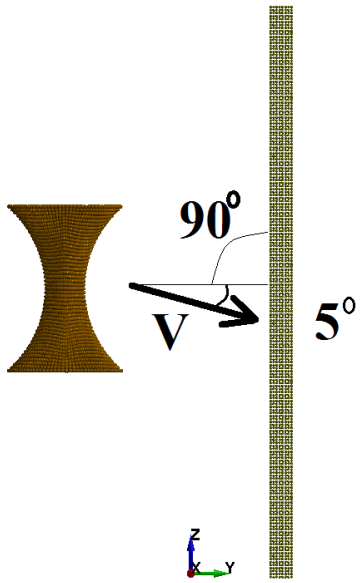

Fig. 19. An impact of paraboloid with a diverted velocity vector at an angle of 5 degrees to barrier normal. Initial condition before calculations t = 0

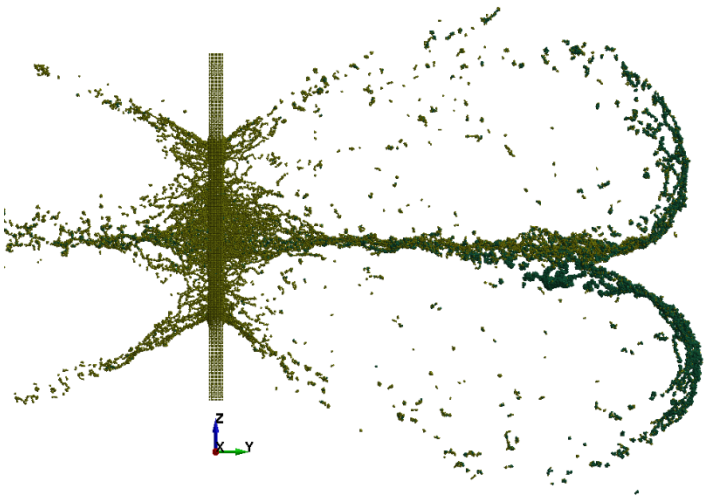

Fig. 20. An impact of paraboloid with a diverted velocity vector at an angle of 5 degrees to barrier normal. Evolution of cloud of debris at t = 10 μs

Figure 20 indicates that qualitative change did not occur in the shape of the cloud. The debris cloud still consists of 2 semi-clouds, we can no longer observe the evident central "spike", however, we see a concentration of mass in the connection point of two semi-clouds.

Consequently, the second important result of the study: in place of contact of two semi-clouds, which emerged from the impact of a paraboloid against a barrier at a speed of 4190 m/s, a significant portion of mass of the debris cloud is concentrated and hence, diverted impact of a solid paraboloid of rotation is as dangerous for the second screen of Whipple shield (after it has passed the first) as an impact of a sphere of equal mass for the first screen of Whipple shield.

Case 2. The velocity vector of paraboloid is at an angle of 5 degrees to barrier normal, the paraboloid itself is rotated 5 degrees so that an angle between paraboloid's rotation axis and impact axis is 90 degrees (Fig. 21).

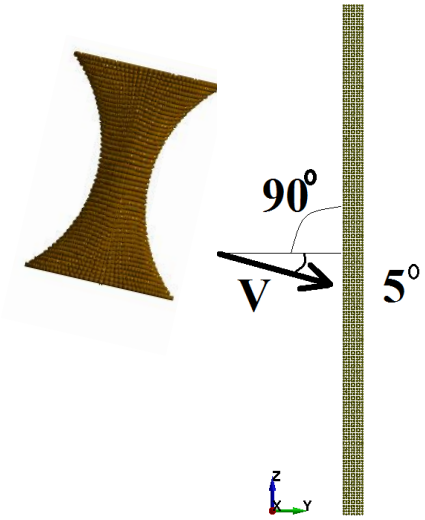

Fig. 21. An impact of paraboloid with a diverted velocity vector at an angle of 5 degrees to barrier normal. Paraboloid is also rotated. Initial condition before calculations, t = 0

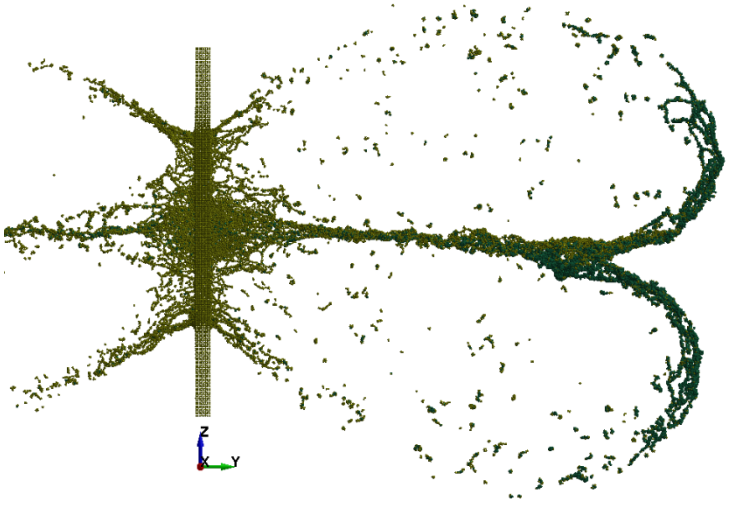

Fig. 22. An impact of paraboloid with a diverted velocity vector at an angle of 5 degrees to barrier normal. Paraboloid is also rotated before impact. Evolution of debris cloud at t = 10 μs

Conclusions of the second case are identical to the first one. No qualitative changes in the shape of the cloud took place compared to the first case. Consequently, there was no significant mass transfer, as we can see from Fig. 22.

Case 3. Velocity vector of paraboloid is at an angle of 30 degrees to barrier normal (Fig. 23).

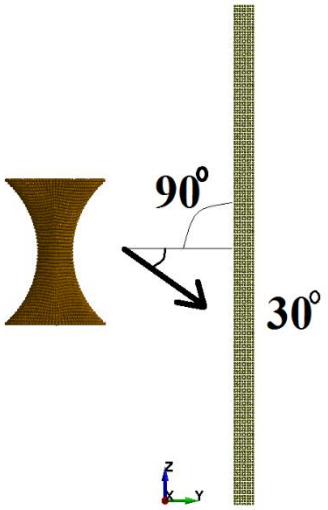

Fig. 23. An impact of paraboloid with a diverted velocity vector at an angle of 30 degrees to barrier normal. Initial condition before calculations t = 0

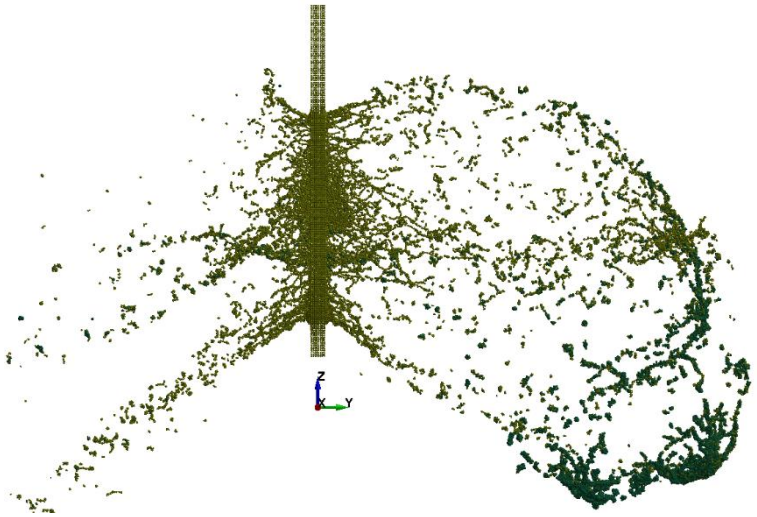

Fig. 24. An impact of paraboloid with a diverted velocity vector at an angle of 30 degrees to barrier normal. Result of numerical simulation at t = 10 μs.

Observing the result of numerical simulation of the case 3 we can see that the "spike" do not appear along the impact axis (Fig. 24), clouds of fragments are forming with evident deflection from symmetry, in vanguard of clouds we witness particles of the striker (shown in dark green).

Diverted impact of paraboloid at an angle of 30 degrees and beyond is significantly less dangerous for the second screen of Whipple shield because, semi-clouds merge in the process of evolution and considerably divert to the side. Therefore, the second screen will be loaded with sliding impact, which is not dangerous.

Case 4. Velocity vector of paraboloid is at an angle of 30 degrees to barrier normal. Paraboloid is rotated to the same angle (Fig. 25).

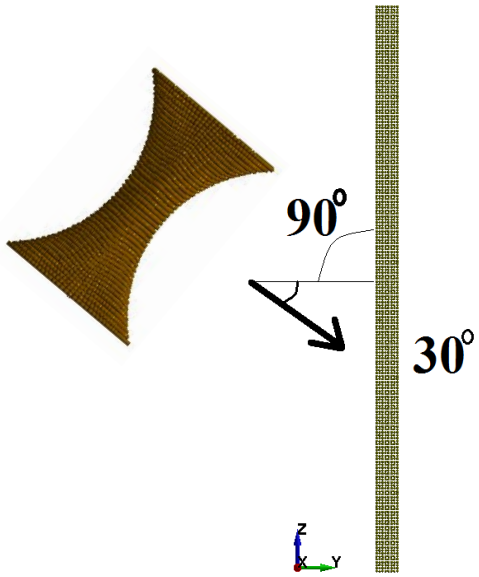

Fig. 25. An impact of paraboloid with a diverted velocity vector at an angle of 30 degrees to barrier normal. Paraboloid is also rotated to the same extent. Initial condition before calculations, t = 0

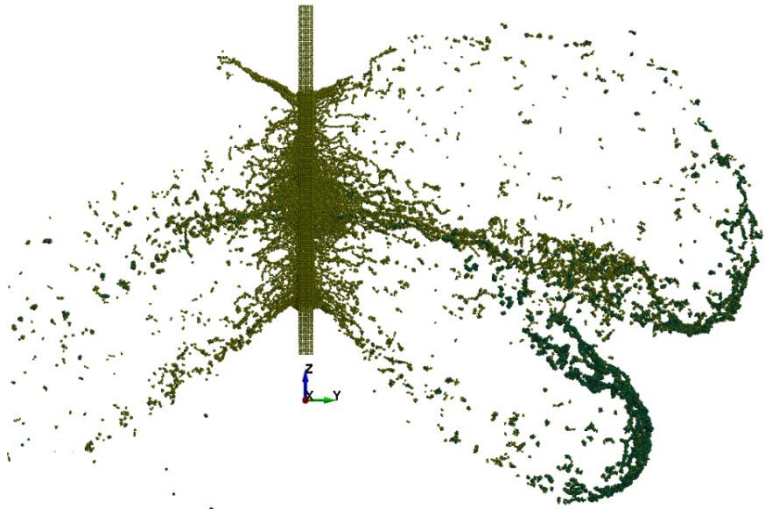

Fig. 26. An impact of paraboloid when both velocity vector and rotation axis are diverted at an angle of 30 degrees to barrier normal. Result of numerical simulation at t = 10 μs

Figure 26 indicates that two semi-clouds do not merge as a result of such impact however, we can clearly see that there is a significant deviation of both semi-clouds from the axis which is perpendicular to the target's surface.

Case 5. Velocity vector of paraboloid is at an angle of 45 degrees to barrier normal (Figure 27).

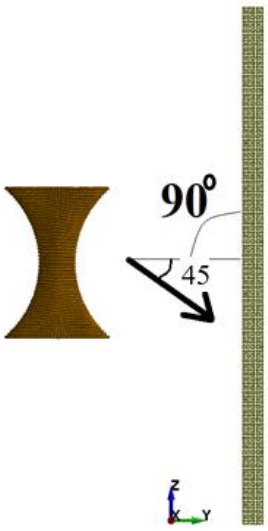

Fig. 27. An impact of paraboloid with a diverted velocity vector at an angle of 45 degrees to barrier normal. Initial condition before calculations t = 0

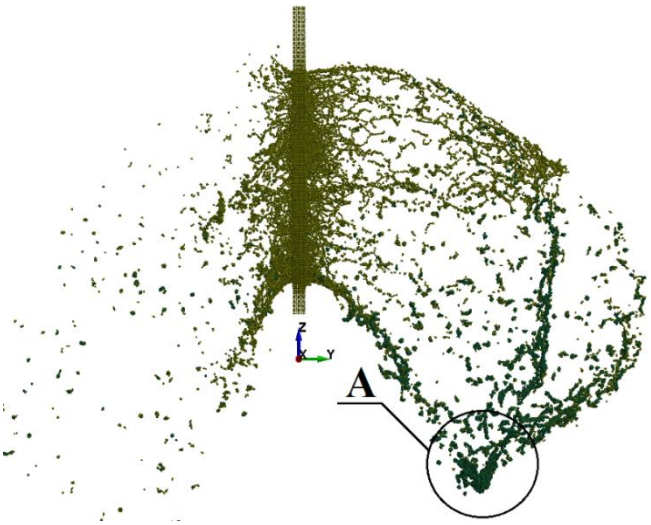

Fig. 28. An impact of paraboloid with a diverted velocity vector at an angle of 45 degrees to barrier normal. Result of numerical simulation at t = 10 μs

Figure 28 indicates that the case of 45 degree divergence is special. In this case, one can see that particles of the cloud concentrate in vanguard A (Fig. 28), and have a movement direction along the surface of the barrier. Such vanguard can pose a threat for stiffening ribs of a spacecraft and other elements which vanguard can meet along the way.

Case 6. Velocity vector of paraboloid is at an angle of 45 degrees to barrier normal (Fig. 29). Paraboloid is rotated to the same angle.

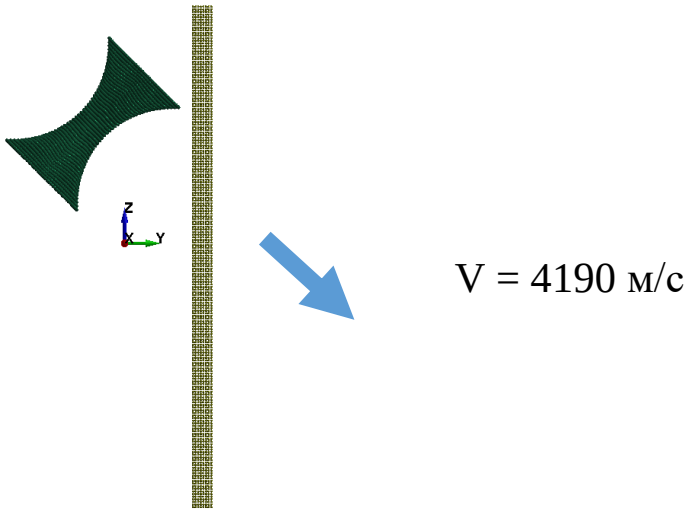

Fig. 29. An impact of paraboloid with a diverted velocity vector at an angle of 45 degrees to barrier normal. Paraboloid is also rotated to the same extent. Initial condition before calculations t = 0

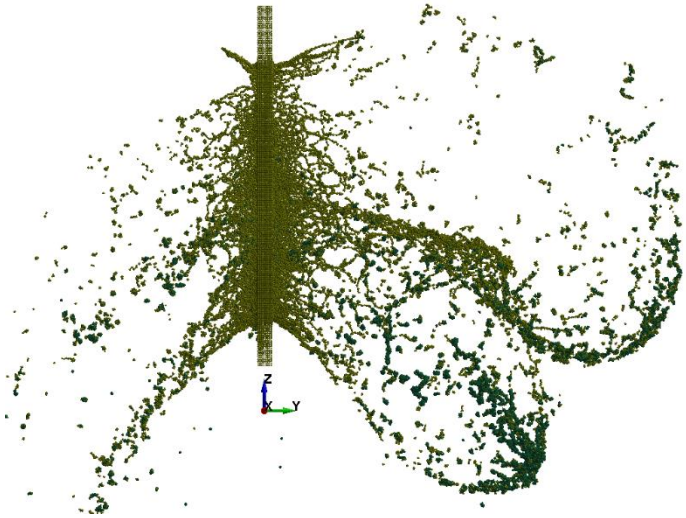

Fig. 30. An impact of paraboloid with a diverted velocity vector at an angle of 45 degrees to barrier normal. Paraboloid is also rotated to the same extent. Results of numerical simulation at t = 10 μs

Thus, in this case one can see that particles do not concentrate in the front of the cloud (Fig. 30), unlike particles in case 5, they have movement direction along the surface of the barrier. And as in case 5 such concentration of fragments is particularly dangerous for stiffeners of a spacecraft and other structural elements.

Results and Discussion

In this article, an impact at high speeds of a solid-paraboloid into a thin aluminum plate was numerically simulated. It was shown in [27] that at velocities of ~ 240 – 750 m/s the nature of aluminum destruction as a result of impact loading is locally-kinetic.

This paper reviews the mechanism of the interaction between the projectile and bumper, the movement and diffusion of the debris cloud, so-called "the effect of mass collapse".

Note that for different collision cases even if all particles of the broken barrier have differently oriented velocity vectors, then they start to gather in reinforced structures and after that they dissociate into smaller ones, in other words, the destruction of the masses begins.

Numerical simulation for high-speed impact of a hyperboloid on an aluminum alloy plate was presented. Central and non-central impacts were considered. It was shown that some types of collisions are very dangerous because significant mass of fragments is concentrated either on the impact axis or along the surface of the barrier.

The case of a normal impact of a paraboloid of rotation into the barrier is very dangerous for the second screen of Whipple shield (relative to the sphere, cube, and other drummers of similar shapes, as was simulated in [22]) because of the particles concentration closer to the axis of impact and their distribution in a rectangle form shown in Fig. 12.

For non-central impact it was shown that particles of the cloud do not concentrate along the impact axis in the front of the cloud (Figs. 28, 30), they have movement direction along the surface of the barrier. This certainly affects the integrity of spacecraft and equipment.

With increasing impact speed, we suppose, a similar process takes place in early stages. That is, after "gathering" of particles into reinforced structures a reverse process takes place – structure crushes, multiple ruptures emerge and clouds of fragments are forming.

References

1. Diki C, Uvarov V. *Novyy Soyuz—Appolon» iz kosmicheskogo musora.* Available from: https://kiozk.ru/article/ekspert/novyj-souz-apollon-iz-kosmiceskogo-musora [Accessed 9th June 2023]. (In-Russin)
2. Whipple FL. Meteorites and space travel. *The Astronomical Journal.* 1947;52: 131.
3. Song Z, Pei X, Yu J, Zhao J, Tan F. Hypervelocity impact tests on a Whipple shield using a flyer plate in the velocity range from 4 km/s to 12 km/s. *Int. J Impact Eng*. 2021;156: 103899.
4. Hayhurst CJ, Clegg RA. Cylindrically symmetric SPH simulations of hypervelocity impacts on thin plates. *Int. J. Impact Eng*. 1997;20(1-5): 337–348.
5. Christiansen EL, Crews JL, Williamsen JE, Robinson JH, Nolen AM. Enhanced meteoroid and orbital debris shielding. *Int. J. Impact Eng*. 1995;17(1-3): 217–228.
6. Hayhurst CJ, Clegg RA. Cylindrically symmetric SPH simulations of hypervelocity impacts on thin plates. *Int. J. Impact Eng*. 1997;20(1–5): 337–348.
7. Hayhurst CJ, Livingstone IH, Clegg RA, Fairlie GE. Numerical Simulation of Hypervelocity Impacts on Aluminum and Nextel/Kevlar Whipple Shields. In: *Proc. Hypervelocity Shielding Workshop, 11 March 1998, Galveston, Texas.* 1998. p.TP031.
8. Panov DV, Silnikov MV, Mikhaylin AI, Rubzov IS, Nosikov VB, Minenko EY, Murtazin DA. Large-scale shielding structures in low earth orbits. *Acta Astronaut*. 2015;109: 153–161.
9. Pierazzo E, Artemieva N, Asphaug E, Baldwin EC, Cazamias J, Coker R, Collins GS, Crawford DA, Davison T, Elbeshausen D, Holsapple KA, Housen KR, Korycansky DG, WÜnnemann K. Validation of numerical codes for impact and explosion cratering: Impacts on strengthless and metal targets. *Meteoritics & Planetary Science*. 2008;43(12): 1917–1938.
10. Christiansen EL. Design and performance equations for advanced meteoroid and debris shields. *Int. J. Impact Eng.* 1993;14: 145–156.
11. Christiansen EL. International Space Station (ISS) Meteoroid/Orbital Debris Shielding. *Cosmonautics and Rocket Engineering.* 2000;18: 166–180.
12. Christiansen EL, Kerr JH. Mesh double-bumper shield: a low-weight alternative for spacecraft meteoroid an orbital debris protection. *Int. J. Impact Eng*. 1993;14: 169–180.
13. Christiansen EL. *Meteoroid/Debris Shielding*. NASA. Report number: TP-2003-210788, 2003.

14. Etemadi E, Zamani J, Francesconi A, Mousavi MV, Giacomuzzo C. A new set-up to investigate plastic deformation of face centered cubic metals in high strain rate loading. *Modern Applied Science*. 2014;8(2): 94–106.
15. Eiceman GA, Karpas Z. *Ion Mobility Spectrometry*. 2nd ed. NY: CRC Press; 2005.
16. Horz F, Cintala MJ, Bernhar RP, See TH. Multiple-mesh bumpers: a feasibility study, *Int. J. Impact Eng*. 1995;17: 431–442.
17. Cherniaev A, Telichev I. Meso-scale modeling of hypervelocity impact damage in composite laminates. *Composites Part B*. 2015;74: 95–103.
18. Parshikov AN, Medin SA. Smoothed particle hydrodynamics using interparticle contact algorithms. *J. Comp. Phys*. 2002;180(1): 358-382.
19. *ANSYS LS-DYNA User's Guide. Release 12.1*. 2009.
20. Cour-Palais BG, Crews JL. A multi-shock concept for spacecraft shielding. *Int. J. Impact Eng*. 1990;10: 135–146.
21. Brandon EJ, Vozoff M, Kolawa EA, Studor GF, Lyons F, Keller MW, Beiermann B, White SR, Sottos NR, Curry MA, Banks DL, Brocato R, Zhou L, Jung S, Jackson TN, Champaigne K. Structural health management technologies for inflatable/deployable structures: Integrating sensing and self-healing. *Acta Astronaut.* 2011;68(7-8): 883–903.
22. Ke F, Huang J, Wen X, Ma Z, Liu S. Test study on the performance of shielding configuration with stuffed layer under hypervelocity impact. *Acta Astronaut*. 2016;127: 553–560.
23. Silnikov MV, Guk IV, Nechunaev AF, Smirnov NN. Numerical simulation of hypervelocity impact problem for spacecraft shielding elements. *Acta Astronaut*. 2018;150: 56–62.
24. Silnikov MV, Guk IV, Mikhaylin AI, Nechunaev AF, Rumyantsev BV. Numerical simulation of hypervelocity impacts of variously shaped projectiles with thin bumpers. *Materials Physics and Mechanics.* 2019;42(1): 20–29.
25. Liu MB, Liu GR. Smoothed Particle Hydrodynamics (SPH): an Overview and Recent Developments. *Arch. Comput. Methods Eng*. 2010;17: 25–76.
26. Liu MB, Liu GR. *Smoothed Particle Hydrodynamics A Meshfree Particle Method*. Singapore: World Scientific Publishing; 2003.
27. Meshcheryakov YI, Konovalov GV, Zhigacheva NI, Divakov AK, Nechunaev AF. Strain Behavior of Aluminum Alloys Under Dynamic Compression and Tensile. *Advanced Structured Materials.* 2022;164: 413–453.
28. Sagomonyan AY. *Pronikaniye.* Moscow: Izdatelstvo Moskovskogo universiteta; 2014. (In-Russian)
29. Wen K, Chen XW, Lu YG. Research and development on hypervelocity impact protection using Whipple shield: An overview. *Defence Technology*. 2021;17(6): 1864-1886.

THE AUTHORS

Nechunaev A.F.
e-mail: vvkgu@yandex.ru

Naumova N.V.
e-mail: n.v.naumova@spbu.ru

Dorofeev N.P.
e-mail: nickdorof60@gmail.com